Ultrafast internal conversion in 4-aminobenzonitrile occurs sequentially along the seam

Pedro J. Castro,[1] Aurelie Perveaux,[2,3] David Lauvergnat,[2] Mar Reguero,[1] and Benjamin Lasorne.[3]

1 Departament de Química Física i Inorgànica, Universitat Rovira i Virgili, 43007, Tarragona, Spain

2 Laboratoire de Chimie Physique (UMR 8000), CNRS, Université Paris-Sud, 91405, Orsay, France

3 Institut Charles Gerhardt (UMR 5253), CNRS, Université de Montpellier, 34095, Montpellier, France

Abstract. Upon UV light absorption, 4-aminobenzonitrile undergoes an ultrafast radiationless decay process from a charge-transfer state to a locally-excited state. This pathway proceeds through an extended seam of conical intersections between the second- and first-excited singlet electronic states. Quantum dynamics simulations show that planar geometries dominate the earlier times (< 20 fs), after which the whole seam becomes explored, as the wavepacket spreads and breathes along both sides of the unstable ridge with respect to the amino-bending coordinate.

1   Introduction

4-aminobenzonitrile (ABN), and its N-dimethyl derivative, DMABN [1] are well-known prototype systems for studying intramolecular charge transfer (ICT) in electron donor/acceptor molecules. Despite their chemical similarity, their luminescent patterns are quite different according to the environment: ABN shows single fluorescence in any solvent (normal band), whereas DMABN exhibits normal fluorescence in non-polar solvents but dual fluorescence in polar ones (normal and anomalous bands) [2, 3]. The sensitivity of ABN derivatives to their environment makes them good

candidates as fluorescent probes, chemical sensors, molecular switches, or electro-optical switches [4, 5, 6, 7, 8].

It is well-established that the normal band is originated from a locally-excited (LE) state, while the anomalous band is due to a charge-transfer (CT) state, with a large dipole moment that is stabilized in polar solvent environments. The exact structure of the species responsible for the anomalous band and the mechanism that populates them are still controversial due to contradictory arguments, based on both experimental observations and theoretical calculations, which support different models and hypotheses [1, 3, 9, 10, 11].

Three received models have been proposed regarding the structure of the luminescent CT species: the planar ICT model (PICT) [12], the twisted one (TICT) [10, 13], and the partially twisted or pretwisted one (pTICT) [14]. It seems sufficiently proven that the PICT and TICT species actually correspond to two minimum-energy points in the potential-energy surface (PES) of the excited CT state in both ABN and DMABN, but their respective roles in the fluorescent spectra remain to be clarified. A fourth model, the rehybridized ICT (RICT) [15], is thought to be a stable species corresponding to a $\pi\sigma^*$ excited state but is nowadays discarded as a luminescent species [16, 17, 18, 19].

The ICT mechanism is triggered upon UV light absorption, which populates first the S_2 state of CT character [20]. The subsequent sequence of steps leading to the S_1 PES (with both LE and CT regions) until the luminescent species are formed is still under discussion. Gómez et al. proposed the following mechanism in 2005 [20]. After excitation to the S_2 state, the

system relaxes to the PICT minimum. The system follows then a barrierless pathway along the amino-bending coordinate to the optimized S_2/S_1 conical intersection (denoted CI-C_s). Because of the extended conical intersection seam, ultrafast radiationless decay from S_2 to S_1 can take place at various torsion angles of the amino group leading either to the LE or the TICT geometries on S_1. Experimental works suggest initial production of the LE species on S_1 through internal conversion from S_2 and later equilibration with a CT species on S_1 [9].

Park et al. reported recently an experimental study based on highly time-resolved fluorescence spectra (TRFS) over the whole emission domain of DMABN in acetonitrile [18]. Such accurate measurements provide valuable information about the dynamics of the ICT process free from the interferences of the solvent reorganization and vibrational relaxation dynamics that occur on the same time scale. The experimental techniques used in that work also give access to an analysis of the ultrafast events that occur within the first few femtoseconds. From their observations it is concluded that, after photoexcitation to the S_2 state (CT), there is significant internal conversion to the S_1 state in less than 30 fs for geometries that are still quasiplanar, thus in the LE region. A similar ultrafast mechanism was also proposed in a previous work by the McCamant group [21, 22].

Computational studies carried out on ABN and DMABN have shown that the topographies of the S_2 and S_1 PESs of both systems are similar, but small energetic changes are suspected to induce a different interplay between the LE and CT species and lead to either normal or dual fluorescence [3, 20]. The initial steps of the deactivation mechanism, though, are expected to be

analogous in both systems, so the experimental conclusions, derived by Park et al. [18] for DMABN, should hold in a qualitative way for ABN as well.

In a previous work [23] on ABN, we have shown that ultrafast production of the LE species in S_1 can occur efficiently via S_2/S_1 internal conversion involving a newly-investigated planar conical intersection (denoted CI-C_{2v}), both in the gas phase and a polar solvent. Although this conical intersection is not the lowest-energy one within the S_2/S_1 intersection seam, it is easily accessible from the Franck-Condon point both geometrically and energetically. In other words, the system is able to deactivate first upon involving coordinates associated to such in-plane skeletal deformations in a first stage, while bending and twisting motions may occur on longer time scales once vibrational energy is redistributed. Curchod et al. did recently a study on DMABN [24] using time-dependent DFT combined with Multiple-Spawning dynamics. While their molecular system (DMABN) is slightly different from ours (ABN), they have reached similar conclusions: ultrafast transfer from S_2 to S_1 can occur without torsion of the amino group.

In the present work, we investigate in more detail the competition between the deactivation pathways through a planar conical intersection, CI-C_{2v}, and through the low-lying C_s one, CI-C_s, so as to provide further information about the ultrafast process that populates the LE state almost immediately after the initial photoexcitation of the CT state. Our objective is to determine whether deactivation occurs specifically around CI-C_{2v}, if the system rather bifurcates early on towards CI-C_s, as suggested by Gómez et al. [20], or if the situation is intermediate, with significant delocalization along the amino-bending coordinate so that the wavepacket will reach the whole portion of the S_1/S_2 seam connecting the bent conical intersection to the planar one at similar times.

2 Computational Details

The topographies of both coupled PESs involved in the initial steps of the process was first determined from a CASSCF(12,11)/cc-pVDZ study using the Gaussian 09 package [25]. Energies in these regions were further refined at the CASPT2 level with the Molcas 7 package [26] so as to include the effect of dynamic correlation in the calculations. In our previous study, we showed that the effect of a polar solvent on ABN only enhances the efficiency of the radiationless decay but does not change the mechanism of the ultrafast process under study (< 30fs) [3, 23]. This was not accounted for in the present study, as calculations *in vacuo* seem sufficient to provide reliable mechanistic information.

In order to run quantum dynamics calculation with the multilayer version [27] of the multiconfiguration time-dependent Hartree (ML-MCTDH) method implemented in the Heidelberg MCTDH package [28, 29], analytical expressions of quasidiabatic coupled PESs are required, often in the form of what is called a vibronic-coupling Hamiltonian (VCH) model [30, 31, 32]. Its entries are expressed usually as linear (linear vibronic-coupling model – LVC) or quadratic (quadratic vibronic-coupling model – QVC) functions of normal Cartesian coordinates originated from the ground-state equilibrium geometry (Franck-Condon point). This is the type of approach that we used in the present work. However, the main originality of our strategy is that we explicitly used analytical relationships between adiabatic data and diabatic parameters so as to obtain the latter automatically. Consistently with our previous study [23], three diabatic states are involved (corresponding

diagonal entries of the electronic-energy matrix: $H_{11}(\mathbf{Q})$, $H_{22}(\mathbf{Q})$, and $H_{33}(\mathbf{Q})$). In addition, along some directions or coordinates, the model was adjusted to obtain a better description of the conical intersections. We thus circumvent numerical fitting procedures that, in some cases, can occur to be time consuming and tedious tasks from a technical perspective. Our full-dimensional models of coupled PESs (39D in the present study) are based on CASSCF energies and geometries and further refined to match CASPT2 data in the gas phase.

The choice of an adequate coordinate system depends on the process under study. In particular, for molecular systems with large-amplitude motions, normal-mode coordinates are not adequate to describe motions leading far from the equilibrium position [33]. Thus, it is often beneficial to describe the molecular system with curvilinear coordinates, *i.e.*, distances and angles, since they describe large-amplitude motions such as for example torsions in a more natural way; in other words, they will provide a simpler expression of the PES. Unfortunately, the use of curvilinear coordinates can lead to very complicated expressions of the kinetic-energy operator (KEO) [34, 35], which can be expressed numerically (but exactly) [36, 37, 38, 39, 40] or analytically [41, 42, 43, 44, 45]. An analytical approach is more practical, as there is no need to compute the numerical the KEO on a grid and then fit the results or make further approximations (for example upon considering Taylor expansions). However, an analytical expression of the KEO is not always compatible with an "MCTDH format" (see below), where operators must be written as sums of products of low-dimensional functions. Some specific types of coordinates allow this condition to be fulfilled, in particular so-called polyspherical coordinates, denoted $\mathbf{Q}_{\text{Poly}}$ [41, 43, 44], which were indirectly used in this study. However, the actual

coordinates, **Q**, used here to define the model and to run the dynamics were obtained after several transformations of the polyspherical coordinates.

2.1 Sets of Coordinates

Fig. 1 depicts the polyspherical vectors and subsystems used to define relative frames (red: S_1; green: $S_{1,1}$; blue: $S_{2,1}$; pink: $S_{1,2,1}$). Subsystems are defined so as to avoid numerical issues related to poles due to collinear vectors (such as $\mathbf{R}_1^{(1)}$ and $\mathbf{R}_2^{(1,1)}$) around the reference geometry [45].
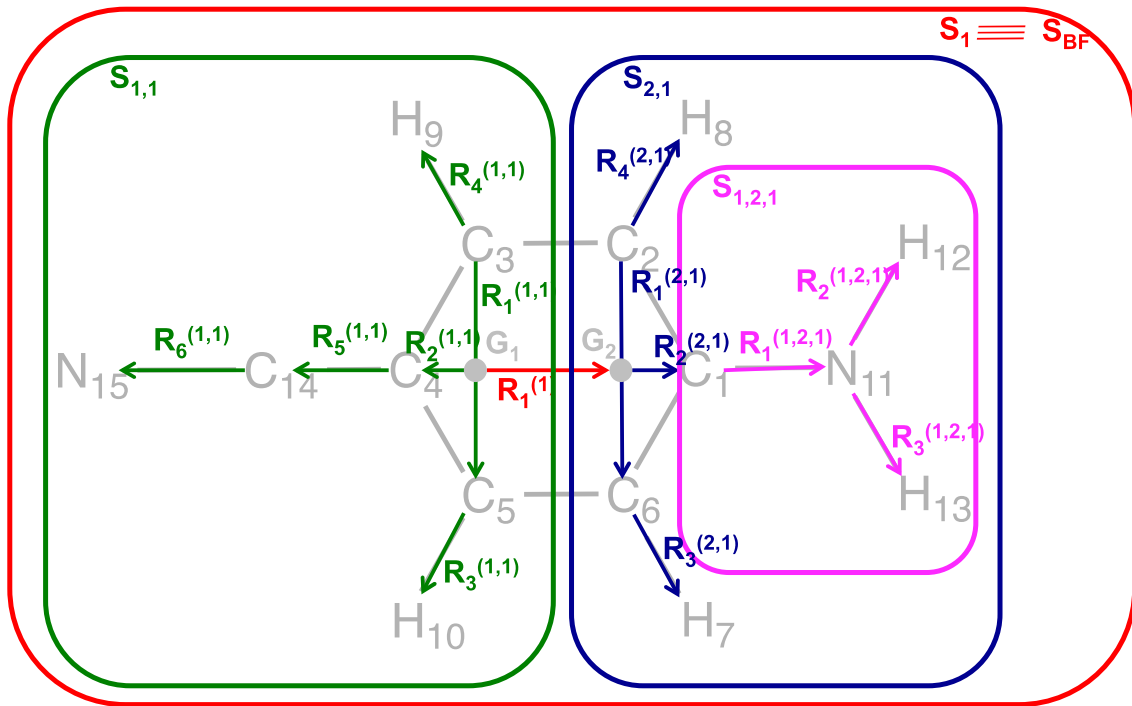
Fig. 1. Polyspherical vectors and subsystems.

Each vector is expressed in terms of spherical coordinates. These coordinates, $\mathbf{Q}_{poly}$, were carefully selected so as to correspond to the most relevant motions involved in the photoprocess. In particular, $R_1^{(1)}$ describes

the quinoidal stretching, $R_2^{(2,1)}$ the symmetric stretching of the allyl-like fragment on the amino side, $\gamma^{(2,1)}$ the envelope ring-puckering on the amino side, $\alpha^{(1,2,1)}$ the pyramidalization of the C-atom attached to the amino group, $\gamma^{(1,2,1)}$ and $\varphi_3^{(1,2,1)}$ the torsion and pyramidalization of the amino group.

Then, two transformations are required: (i) the polyspherical coordinates, $\mathbf{Q}_{\text{poly}}$, are symmetrized with respect to the C_{2v} point group (see Table 1); such symmetrized coordinates, $\mathbf{Q}_{\text{sym}}$, make it possible to enforce C_{2V} symmetry into *ab-initio* data (Hessians, gradients) obtained numerically; (ii) effective coordinates are defined from a linear transformation of $\mathbf{Q}_{\text{sym}}$ such that a single coordinate is defined according to each conical-intersection direction (Eq. 1). The remaining linear combinations belong to the orthogonal complement. This coordinate change is performed automatically with the T_{NUM} program that uses the vectors $\mathbf{R}_{22}^{\text{LE}}$ and $\mathbf{R}_{33}^{\text{PICT}}$ expressed in terms of the symmetrized coordinates,

$$\mathbf{R}_{22}^{\text{LE}} = \frac{\mathbf{Q}_{\text{sym}_{\text{CI}-\text{C}_{2v}}} - \mathbf{Q}_{\text{sym}_{\text{LE}}}}{\left\|\mathbf{Q}_{\text{sym}_{\text{CI}-\text{C}_{2v}}} - \mathbf{Q}_{\text{sym}_{\text{LE}}}\right\|},$$

$$\mathbf{R}_{33}^{\text{PICT}} = \frac{\mathbf{Q}_{\text{sym}_{\text{CI}-\text{C}_{2v}}} - \mathbf{Q}_{\text{sym}_{\text{PICT}}}}{\left\|\mathbf{Q}_{\text{sym}_{\text{CI}-\text{C}_{2v}}} - \mathbf{Q}_{\text{sym}_{\text{PICT}}}\right\|},$$

Eq. 1

where $\mathbf{Q}_{\text{sym}_{\text{LE}}}$ and $\mathbf{Q}_{\text{sym}_{\text{PICT}}}$ are the PICT or the LE minima, respectively, and $\mathbf{Q}_{\text{sym}_{\text{CI}-\text{C}_{2v}}}$ is the geometry of C_{2v} conical intersection.

Table 1. Variations of the original set of polyspherical coordinates ($\Delta \mathbf{Q_{Poly}} = \mathbf{Q_{Poly}} - \mathbf{Q_{Poly_0}}$) symmetrized with respect to a planar C$_{2v}$ reference geometry ($\mathbf{Q_{Poly}} = \mathbf{Q_{Poly_0}}$). In this, we used a convention where (*zy*) is the molecular plane (‖) and (*zx*) is the perpendicular plane (⊥). $\boldsymbol{A_2}$ deformations are torsions, $\boldsymbol{B_2}$ deformations are in-plane left-right-breaking motions, and $\boldsymbol{B_1}$ deformations are out-of-plane up-down-breaking motions.

$A_1\ [C_{2v} \Rightarrow C_{2v}]$	$A_2\ [C_{2v} \Rightarrow C_2]$	$B_1\ [C_{2v} \Rightarrow C_s^{\perp}]$	$B_2\ [C_{2v} \Rightarrow C_s^{\parallel}]$
$\Delta R_1^{(1)}$	$\dfrac{\Delta\varphi_4^{(1,1)} - \Delta\varphi_3^{(1,1)}}{2}$	$\dfrac{\Delta\varphi_4^{(1,1)} + \Delta\varphi_3^{(1,1)}}{2}$	$\dfrac{\Delta R_4^{(1,1)} - \Delta R_3^{(1,1)}}{2}$
$\Delta R_1^{(1,1)}$	$\dfrac{\Delta\varphi_4^{(2,1)} - \Delta\varphi_3^{(2,1)}}{2}$	$\Delta\varphi_5^{(1,1)}$	$\dfrac{\Delta R_4^{(2,1)} - \Delta R_3^{(2,1)}}{2}$
$\Delta R_2^{(1,1)}$	$\Delta\gamma^{(1,2,1)} + \dfrac{\Delta\varphi_3^{(1,2,1)}}{2}$	$\Delta\varphi_6^{(1,1)}$	$\dfrac{\Delta R_3^{(1,2,1)} - \Delta R_2^{(1,2,1)}}{2}$
$\dfrac{\Delta R_4^{(1,1)} + \Delta R_3^{(1,1)}}{2}$	$\Delta\alpha^{(2,1)}$	$\dfrac{\Delta\varphi_4^{(2,1)} + \Delta\varphi_3^{(2,1)}}{2}$	$\Delta\theta_2^{(1,1)}$
$\Delta R_5^{(1,1)}$		$\Delta\varphi_3^{(1,2,1)}$	$\dfrac{\Delta\theta_4^{(1,1)} + \Delta\theta_3^{(1,1)}}{2}$
$\Delta R_6^{(1,1)}$		$\Delta\alpha^{(1,2,1)}$	$\Delta\theta_5^{(1,1)}$
$\Delta R_1^{(2,1)}$		$\Delta\gamma^{(1,1)}$	$\Delta\theta_6^{(1,1)}$
$\Delta R_2^{(2,1)}$		$\Delta\gamma^{(2,1)}$	$\Delta\theta_2^{(2,1)}$
$\dfrac{\Delta R_4^{(2,1)} + \Delta R_3^{(2,1)}}{2}$			$\dfrac{\Delta\theta_4^{(2,1)} + \Delta\theta_3^{(2,1)}}{2}$
$\Delta R_1^{(1,2,1)}$			$\dfrac{\Delta\theta_3^{(1,2,1)} - \Delta\theta_2^{(1,2,1)}}{2}$
$\dfrac{\Delta R_3^{(1,2,1)} + \Delta R_2^{(1,2,1)}}{2}$			$\Delta\beta^{(1,1)}$
$\dfrac{\Delta\theta_4^{(1,1)} - \Delta\theta_3^{(1,1)}}{2}$			$\Delta\beta^{(2,1)}$
$\dfrac{\Delta\theta_4^{(2,1)} - \Delta\theta_3^{(2,1)}}{2}$			$\Delta\beta^{(1,2,1)}$
$\dfrac{\Delta\theta_3^{(1,2,1)} + \Delta\theta_2^{(1,2,1)}}{2}$			

2.2 Quasidiabatic Model of Coupled PESs

The quasidiabatic PESs and couplings are represented as a 3×3 electronic Hamiltonian matrix based on a generalization of the VCH model [30]. It consists in a real symmetric matrix, $\mathbf{H}(\mathbf{Q})$, made of three diagonal potential-energy functions, $H_{11}(\mathbf{Q}), H_{22}(\mathbf{Q})$, and $H_{33}(\mathbf{Q})$, and three off-diagonal electronic couplings, $H_{12}(\mathbf{Q}), H_{13}(\mathbf{Q})$, and $H_{23}(\mathbf{Q})$. In the Franck-Condon region the three diabatic states are chosen to correlate with the adiabatic ones: state 1 (S_0/GS), state 2 (S_1/LE), and state 3 (S_2/CT).

The non-adiabatic coupling terms between S_0 and the other two states can be neglected. In other words, $H_{11}(\mathbf{Q})$ is identified to the S_0 PES and the electronic couplings $H_{12}(\mathbf{Q})$ and $H_{13}(\mathbf{Q})$ are set to zero. The remaining coupling, $H_{23}(\mathbf{Q})$, is expanded linearly around $\mathbf{Q}_{\text{CI-}C_{2v}}$, the geometry of the C_{2v} conical intersection between S_1 and S_2, along the derivative coupling calculated at this point. The derivative couplings at both the CI-C_{2v} and the CI-C_s points are very similar and correspond essentially to a B_2/A'' Kekulé-like motion that breaks the left/right symmetry of the molecule, and which does not change much all over the seam as illustrated on Fig. 2.
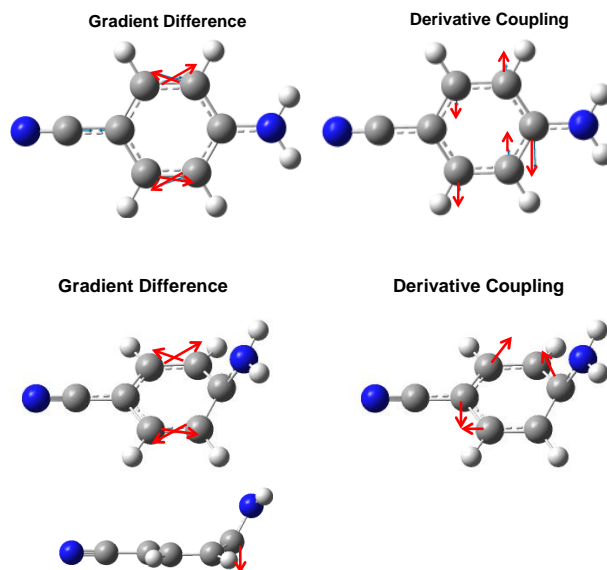
Fig. 2. Gradient differences and derivative couplings at CI-C_{2v} (upper panel) and CI-C_s (lower panel) calculated at the CASSCF(12,11)/cc-pVDZ level of theory with 0.5:0.5 state-averaging on S_1 and S_2.

Note that our procedure can define the gradient of the electronic coupling as any linear combination of the two vectors of the branching space rotated together such that $H_{23}(\mathbf{Q}_0) = 0$ where $\mathbf{Q}_0$ is some chosen geometry where the states are not degenerate. This point is used as a reference for setting the value of the arbitrary mixing angle between both degenerate states at the conical intersection. The extra condition thus implies that the adiabatic and quasidiabatic representations coincide at $\mathbf{Q}_0$. Here, symmetry guarantees that $H_{23}(\mathbf{Q}) = 0$ at all C_{2v}/C_s points (*i.e.*, as long as there is no distortion along $B_2/A"$ modes). For example, $H_{23}(\mathbf{Q}_{\text{PICT}}) = 0$. In practice, the $B_2/A"$ derivative coupling is identified to the gradient of the electronic coupling in the present situation.

As a starting approximation, each diagonal entry was expanded as a quadratic form, $H_{ii}(\mathbf{Q}) \approx H_{ii}^{\text{quad}}(\mathbf{Q})$ with $i = 1,2,3$, around a reference

11

geometry, $\mathbf{Q}_{\mathrm{ref},ii}$, corresponding to the relevant C$_{2v}$ stationary point: $\mathbf{Q}_{\mathrm{GS}} = \mathbf{Q}_{\mathrm{ref},11}$, $\mathbf{Q}_{\mathrm{LE}} = \mathbf{Q}_{\mathrm{ref},22}$, and $\mathbf{Q}_{\mathrm{PICT}} = \mathbf{Q}_{\mathrm{ref},33}$. The quasidiabatic curvatures of the diagonal entries, $H_{ii}^{\mathrm{quad}}(\mathbf{Q})$, were obtained from the adiabatic ones at those points through a second-order Jahn-Teller procedure (whereby the difference between the adiabatic and quasidiabatic second derivatives is considered as a second-order effect involving the non-adiabatic coupling).

In a second stage, the curvatures along the two directions $\mathbf{Q}_{\mathrm{LE}} - \mathbf{Q}_{\mathrm{CI\text{-}C}_{2v}}$ (proportional to $\mathbf{R}_{22}^{\mathrm{LE}}$, see Eq. 1) and $\mathbf{Q}_{\mathrm{PICT}} - \mathbf{Q}_{\mathrm{CI\text{-}C}_{2v}}$ (proportional to $\mathbf{R}_{33}^{\mathrm{PICT}}$, see Eq. 1) were slightly adjusted to enforce that the two quasidiabatic PESs $H_{22}(\mathbf{Q})$ and $H_{33}(\mathbf{Q})$ crossed exactly at $\mathbf{Q}_{\mathrm{CI\text{-}C}_{2v}}$ and did so with the right energy. Fig. 3 shows the agreement between the *ab-initio* energies and those of our VCH model (based on CASPT2 data in the gas phase) for a cut along the direction $\mathbf{Q}_{\mathrm{PICT}} - \mathbf{Q}_{\mathrm{CI\text{-}C}_{2v}}$.
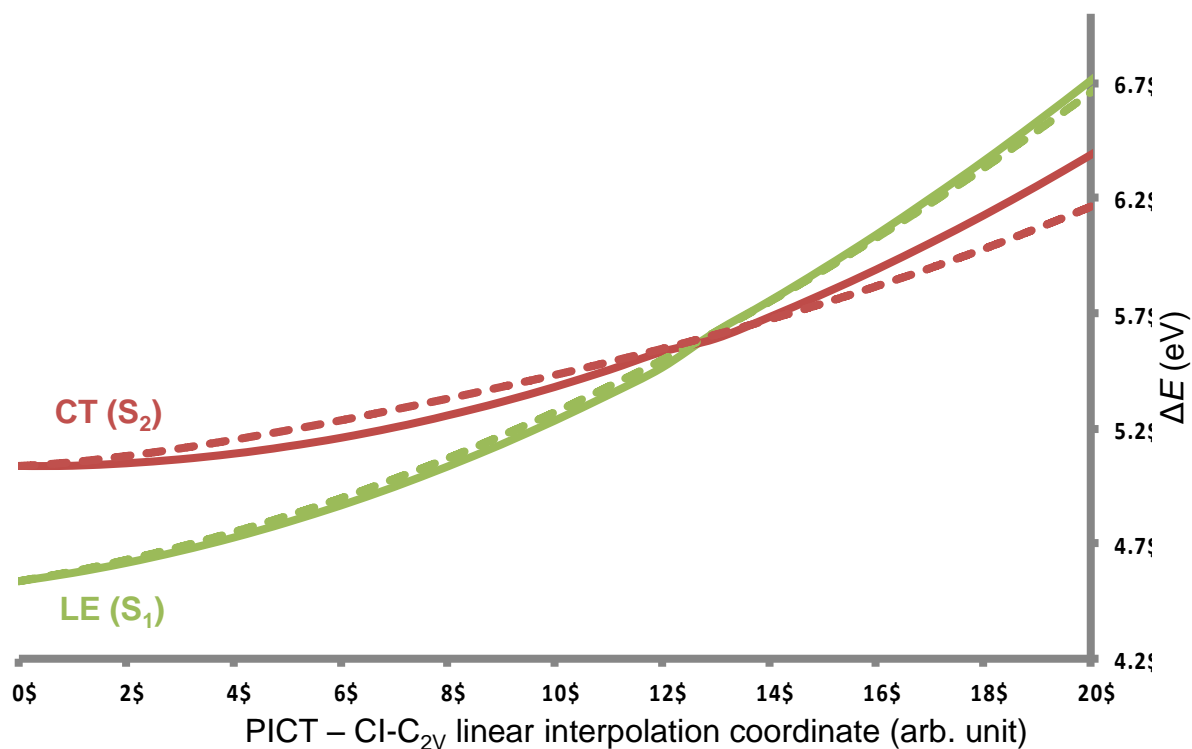
Fig. 3. C_{2v} pathway along a linear-interpolation coordinate Q linking the PICT point (Q = 0) to the CI-C_{2v} point (Q = 13). Energy differences are given with respect to the ground-state minimum. Dashed lines: *ab initio*; plain lines: model. *Ab-initio* level of theory: CASPT2/cc-pVDZ and MS2-CASPT2 at the CI-C_{2v} point.

In addition, accessing the bent conical intersection (CI-C_s) requires breaking the C_{2v} symmetry of the molecule along the non-totally-symmetric bending motion of the amino group, $\alpha^{(1,2,1)}$. This coordinate, the first Euler angle of the sub-system (1,2,1), describes the motion of the amino group (see Fig. 1). In other words, there is a pair of equivalent bent conical intersections, denoted CI-C_s^+ and CI-C_s^-, where the amino group is either up or down with respect to the molecular plane, as shown on Fig. 4.
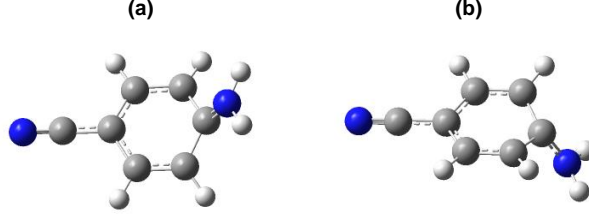
Fig. 4. Optimized geometry at the CASSCF(12,11)/cc-pVDZ level of theory of the pair of S_2/S_1 conical intersections denoted CI-$\mathbf{C}_s^+$ (a) and CI-$\mathbf{C}_s^-$ (b).

To account for the instability of the C_{2v} pathway (see Fig. 5), we refined the expression of $H_{ii}(\mathbf{Q})$ (see Eq. 2) for $i = 2,3$ upon using a switch-type function denoted F_{switch} (see Eq. 3). Its purpose is to modify symmetrically the curvature with respect to the amino-bending coordinate, x (x is one of the coordinates $\mathbf{Q}$), and enforce that $H_{22}(\mathbf{Q})$ and $H_{33}(\mathbf{Q})$ intersect exactly at $\mathbf{Q}_{\text{CI-C}_S^+}$ and $\mathbf{Q}_{\text{CI-C}_S^-}$ with the right energy. The switch-modified diagonal quasidiabatic PESs and $\check{f}_{ii}$, the new curvatures that controls the conical intersection (CI-C_S^+ and CI-C_S^-) energies, read:

$$H_{ii}(\mathbf{Q}) = H_{ii}^{\text{quad}}(\mathbf{Q}) \qquad\qquad \text{Eq. 2}$$

$$+ \frac{1}{2}\check{f}_{ii}\left(F_{\text{switch}}(x) - F_{\text{switch}}(0)\right)\left(\frac{\tanh(0.5 \cdot x)}{0.5}\right)^2.$$

The value of $\check{f}_{ii}$ is obtained at $\mathbf{Q}_{\text{CI-C}_S^+}$ and thus at $x_{\text{CI-C}_S^+}$ (or $\mathbf{Q}_{\text{CI-C}_S^-}$ and $x_{\text{CI-C}_S^-}$) upon imposing $H_{ii}\left(\mathbf{Q}_{\text{CI-C}_S^+}\right) = V\left(\mathbf{Q}_{\text{CI-C}_S^+}\right)$ in Eq. 2, where $V\left(\mathbf{Q}_{\text{CI-C}_S^+}\right)$ is the *ab-initio* energy of the conical intersection at $\mathbf{Q}_{\text{CI-C}_S^+}$,

$$F_{\text{switch}}(x) = \frac{1 + \tanh\left(x - \frac{x_{\text{CI-C}_\text{S}^+}}{2}\right)}{2} + \frac{1 - \tanh\left(x + \frac{x_{\text{CI-C}_\text{S}^+}}{2}\right)}{2}. \qquad \text{Eq. 3}$$

Fig. 5 shows the agreement between the *ab-initio* energies and those of our VCH model (based on CASPT2 data in the gas phase) along the amino-bending direction. The largest difference between the *ab-initio* data and the model is 0.04 eV, which is within the range of error for high-level *ab-initio* methods.
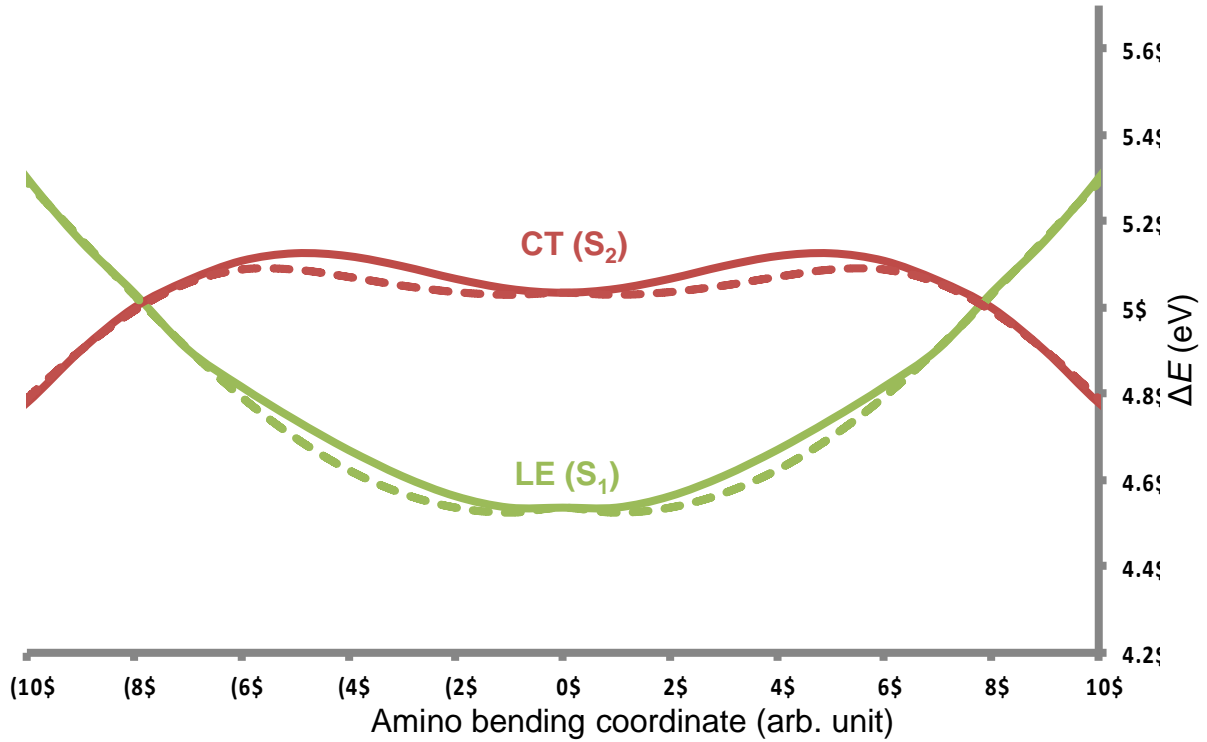
Fig. 5. C_s pathway along a linear-interpolation coordinate Q linking the PICT point (Q = 0) to the pair of CI-C_s^+ and CI-C_s^- points (Q = +8 and –8). Energy differences are given with respect to the ground-state minimum. Dashed lines: *ab initio*; plan lines: model. *Ab-initio* level of theory: CASPT2/cc-pVDZ and MS2-CASPT2 at the CI-$C_s^{+/-}$ points.

2.3 ML-MCTDH

The principle of the MCTDH method is the use of the following wavefunction *ansatz*, Eq. 4, to solve the time-dependent Schrödinger equation for a system with M degrees of freedom, $\mathbf{Q} = [Q_1 \cdots Q_M]$. The nuclear wavefunction is expanded in terms of time-dependent direct products of orthonormal time-dependent Single Particle Functions (SPFs), denoted $\varphi_{j_K}^{(K)}$, where both the coefficients and the basis functions are optimized (as in an MCSCF electronic wavefunction),

$$\psi^{\text{nuclear}}(Q_1, \cdots Q_M, t) = \sum_{j_1=1}^{n_1} \cdots \sum_{j_M=1}^{n_M} A_{j_1,\ldots,j_M}(t) \prod_{K=1}^{M} \varphi_{j_K}^{(K)}(Q_K, t). \qquad \text{Eq. 4}$$

The SPFs are themselves expanded in terms of primitive basis functions,

$$\varphi_{j_K}^{(K)}(Q_K, t) = \sum_{v_K=1}^{N_K} C_{j_K;v_K}^{(K)}(t)\, \chi_{v_K}^{(K)}(Q_K). \qquad \text{Eq. 5}$$

Therefore, MCTDH can be seen as a two-layer scheme with time-dependent coefficients: $A_{j_1,\ldots,j_M}(t)$ at the top layer, and sets of second-layer time-dependent coefficients $C_{j_K;v_K}^{(K)}(t)$ for each degree of freedom.

The size of the SPF basis can be further reduced by combining the physical coordinates $[Q_1 \cdots Q_M]$ into logical coordinates (also called combined modes) $[\mathbf{Q}_1^1 \cdots \mathbf{Q}_P^1]$, such that each logical coordinate, $\mathbf{Q}_K^1$, comprises one or several of the physical coordinates, as $\mathbf{Q}_K^1 = [Q_{1_K} \cdots Q_{d_K}]$. The superscript 1 in the notation represents the layer number of the combined modes (notation introduced to make explicit the multilayer formulation).

The MCTDH nuclear wavefunction with combined modes reads

$$\psi^{\text{nuclear}}\left(\mathbf{Q}_1^1, \cdots \mathbf{Q}_P^1, t\right) = \sum_{j_1=1}^{n_1} \cdots \sum_{j_P=1}^{n_P} A_{1;j_1,\dots,j_P}^1(t) \prod_{K=1}^{P} \varphi_{j_K}^{(1;K)}\left(\mathbf{Q}_K^1, t\right). \qquad \text{Eq. 6}$$

The time-dependent basis functions $\varphi_{j_K}^{(1;K)}$ are now multidimensional. Introducing mode combination implies that the computational effort is transferred from the propagation of a large vector of $A_{1;j_1,\dots,j_P}^1(t)$ coefficients with one-dimensional SPFs, to a shorter vector of coefficients but multidimensional SPFs. Some experience and knowledge of the system under study is required to find an efficient mode-combination scheme for the study. For example, combining modes with similar frequencies is a possible strategy, as shown by O. Vendrell *et al.* [27].

The mode-combined SPFs expressed in the primitive basis are given by

$$\varphi_{j_K}^{(1;K)}\left(\mathbf{Q}_K^1, t\right) = \sum_{v_{1_K}}^{N_{1_K}} \cdots \sum_{v_{d_K}}^{N_{d_K}} C_{j_K;v_{1_K}\dots v_{d_K}}^{(2;K)}(t) \prod_{i=1}^{d_K} \chi_{v_{i_K}}^{(K,i_K)}(\mathbf{Q}_{i_K}). \qquad \text{Eq. 7}$$

In a high-dimensional system one should combine groups of degrees of freedom into high-dimensional SPFs in order to make the size of the vector of coefficients in Eq. 6 manageable (*i.e.*, to get a wavefunction propagation that is reasonable in terms of computation time). However, the combined SPFs are too large to be efficiently propagated. The ML-MCTDH layering scheme is a very flexible way of dealing with this issue. One treats the combined mode as a "sub-configuration" involving smaller groups of logical coordinates. This introduces a new layer of coefficients, the size of which is manageable. The procedure can be repeated over and over until the primitive degrees of freedom are reached.

According to standard use, we may refer to the one-layer scheme as the standard method (primitive basis), to the two-layer scheme simply as MCTDH, and to deeper layering schemes as ML-MCTDH.

Our system, consisting in 39 nuclear coordinates, was described with up to a five-layer wavefunction, and for each layer eight SPFs were used except for the last layer. For the primitive basis sets (the so-called last layer) we used, as usual, the discrete variable representation (DVR) with 40 grid points corresponding to harmonic-oscillator basis sets. The vibrational ground state on S_0 was obtained with the relaxation procedure implemented for the ML-MCTDH method.

As shown in the previous section, to adjust the linear vibronic-coupling model, the coordinates used in the dynamics are defined as linear combinations of polyspherical coordinates. Therefore, the analytical KEO is not simply expressed as a sum of products and it cannot be used with MCTDH directly. To overcome this difficulty and with the help of TNUM [38], we generated a Taylor expansion of the metric tensor, $\mathbf{G}(\mathbf{Q})$, around the reference geometry of S_0. In this study, we only used a zero-order approximation. In other words, the $\mathbf{G}$-matrix will be considered constant all over the coordinate grid.

3   Results and Discussion

Fig. 6 shows a comparison of the evolution of the quasidiabatic populations obtained with: (i) our previous model [23], essentially focused on the description of the deactivation pathway through the C_{2v} conical

intersection; (ii) the present model, which also describes correctly the C$_{2v}$-breaking motion along the amino-bending direction that leads to the C$_s$ conical intersection.

It shall be noted that the generalised VHC model and the quantum simulations in the present study enable to describe only the short-time (sub-picosecond) internal-conversion process. In addition, in order for the system to return to the low-lying electronic state and thus reach thermal equilibrium, other processes must be taken into account, such as other internal-conversion mechanisms, internal vibrational redistribution, fluorescence, solvent effect...
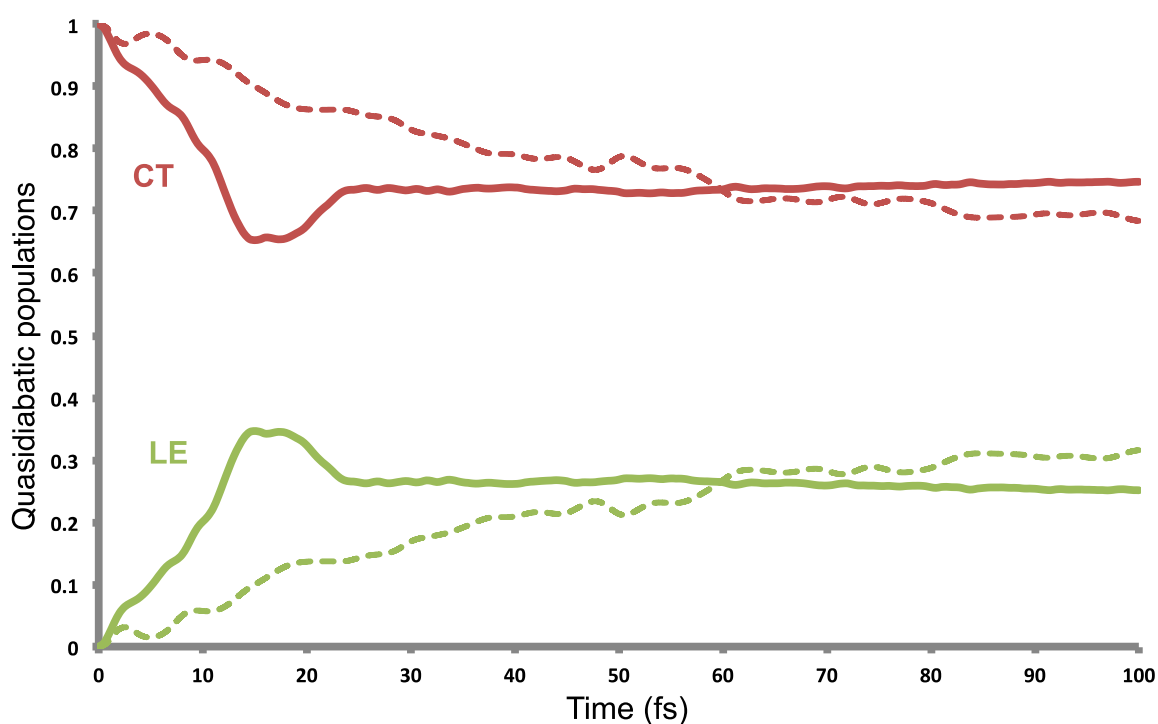
Fig. 6. Time evolution of the quasidiabatic populations of the LE and CT electronic states in the gas phase. Coupled PES model based on CASPT2 data. Plain line: model describing both bent and planar deactivation pathways; dashed line: model describing the planar deactivation pathway [23].

One can notice that the transfer of quasidiabatic population between the CT and LE electronic states is faster when both deactivation pathways are described on the same footing (plain line) but it becomes similar on longer time scales (after 50-100 fs).

However, this result is global and does not discriminate the relative efficiencies and roles of the two different conical intersections (*i.e.*, CI-C$_s$ and CI-C$_{2v}$) with respect to the deactivation process. To this end, we defined different regions along the amino-bending coordinate, centred on each conical intersection and with borders located midway between CI-C$_{2v}$ and CI-C$_s^{+/-}$. The partial populations integrated within these regions will be called local quasidiabatic populations (for each specific conical intersection) and their time evolutions are presented in Fig. 7 for the LE state.
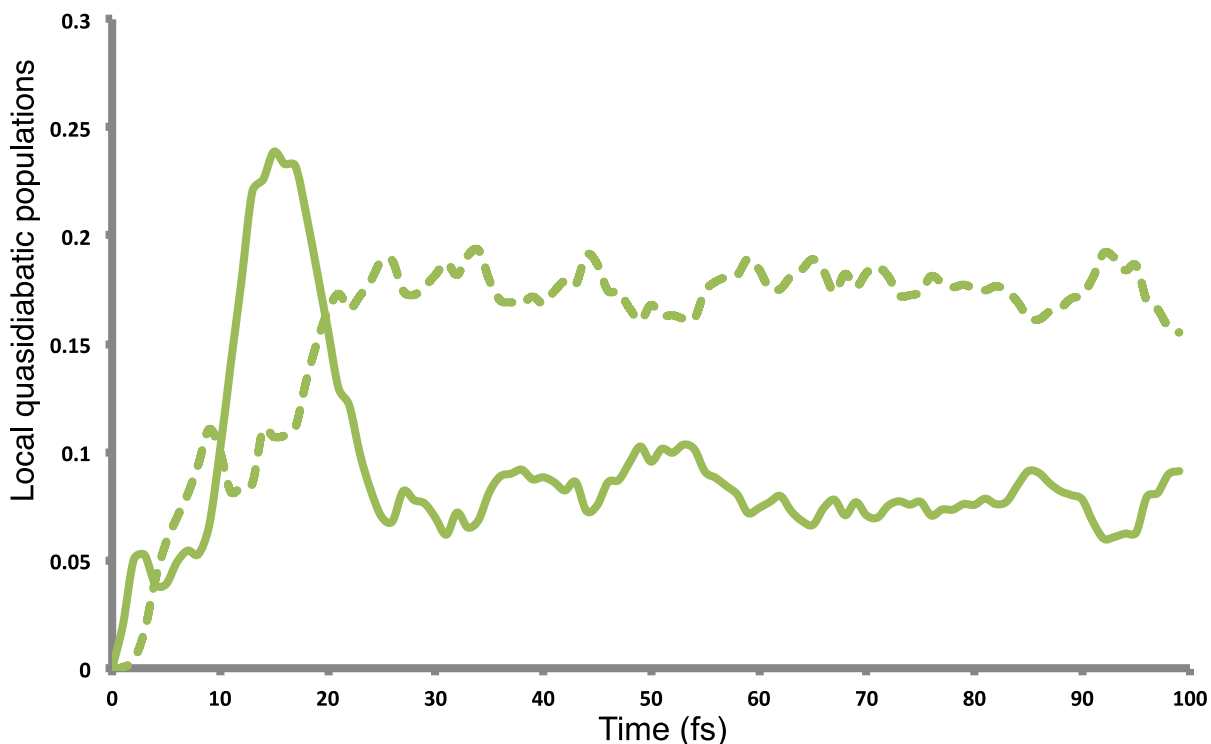
Fig. 7. Time evolution of the local quasidiabatic populations transferred to the LE state in the gas phase. Coupled PES model based on CASPT2 data. Plain line: local population

transferred around CI-C$_{2v}$; dashed line: local population transferred around both CI-C$_s^+$ and CI-C$_s^-$.

The evolution of the local quasidiabatic populations within the inner (around CI-C$_{2v}$) and outer (around CI-C$_s^{+/-}$) regions shows two sequences. The first sequence concerns times less than 20fs: the transfer of population occurs mainly in the vicinity of CI-C$_{2v}$ (sharp peak corresponding to a maximum of 24% of population transferred to LE around CI-C$_{2v}$ whereas population transferred around both CI-C$_s^+$ and CI-C$_s^-$ increases more smoothly, up to 16% within the same period of time; see Fig. 7). After 20 fs, the local quasidiabatic population within the outer region becomes larger and evolves as a mirror image of the local quasidiabatic population within the inner region. One can notice that the global quasidiabatic population no longer evolves after about 25 fs (green plain line in Fig. 6). This indicates that the width of the wavepacket has now increased enough for both regions to be populated significantly and only exhibits a slight oscillatory breathing along the amino-bending direction. In summary, the non-adiabatic transfer of population occurs sequentially along the seam. Before 20 fs, the wavepacket travels on a ridge along the planar deactivation channel with no significant spreading. After 20 fs, delocalization along the amino-bending coordinate implies that the whole seam is reached. Comparison with the results our previous simulations shows that accounting for this spreading makes the transfer of population a bit faster but not more efficient overall.

4 Conclusions

In this study, we have performed quantum dynamics simulations on ABN in the gas phase in order to describe the competition between two deactivation pathways from the initially-excited S_2 state to the luminescent S_1 state and provide further information about the ultrafast process that populates the LE state almost immediately after the initial photoexcitation.

We have developed a full-dimensional (39D) quasidiabatic model of coupled PESs based on CASSCF(12,11)/cc-pVDZ data further refined to match to CASPT2 data in the gas phase. This model, which describes the whole portion of the S_2/S_1 deactivation seam along the amino-bending coordinate, was used to run quantum dynamics simulations with ML-MCTDH.

Our quantum dynamics calculations clearly indicate that deactivation is first localized around the planar conical intersection (CI-C_{2v}) and becomes delocalized after about 20 fs along the S_2/S_1 seam connecting the pair of lower-energy amino-bent conical intersections (CI-C_s^+ and CI-C_s^-) to the planar one (centre of the seam). The PICT species on S_2 is populated right after photoexcitation where it undergoes internal conversion to the LE species on S_1 very early, mainly through the planar conical intersection. The amino-bending motion is not crucial for the overall efficiency of the internal conversion. However, delocalization of the wavepacket along the amino-bending direction implies that the wavepacket explores a larger portion of the seam, which makes the deactivation process faster. Such computational results are consistent with the recent theoretical work of Curchod et al. on the parent system DMABN [24] and the recent experimental observation of

Park et al. [18] in DMABN as well where the first deactivation step is attributed to quasiplanar motions inducing ultrafast internal conversion and direct formation of the LE species in less than 30 fs.

As shown in our previous study [23], this feature is expected to be even more efficient in polar solvents than in the gas phase due to the strong stabilization of the CT state with respect to the LE state, which results in making the conical intersections closer to the Franck-Condon region.

5   Acknowledgements

References:

[1] Z. R. Grabowski, K. Rotkiewicz, and W. Rettig Chem. Rev. 103 (2003) 3899-4031 and references therein. DOI: 10.1021/cr940745l

[2] W. Rettig, Angew. Chem. Int., 25 (1986) 971–988. DOI: 10.1002/anie.198609711

[3] Isabel Gómez, Pedro J. Castro, and Mar Reguero, J. Phys. Chem. A ,119 (2015) 1983–1995. DOI: 10.1021/acs.jpca.5b01421

[4] C.-C. Lin, C.-L. Chen, M.-W. Chung, Y.-J. Chen, P.-T. Chou, J. Phys. Chem. A 114 (2010) 10412-10420.

[5] J. R. Lakowicz, Principles of Fluorescence Spectroscopy, 3rd Edition, Springer US, Editor, 2006. DOI: 10.1007/978-0-387-46312-4

[6] M. Bedoya, G. Orellana, M. C. Moreno-Bondi, Helv. Chim. Acta 84 (2001) 2628-2639. DOI: 10.1002/1522-2675(20010919)84:9<2628::AID-HLCA2628>3.0.CO;2-O

[7] A. P. de Silva, H. Q. N. Gunaratne, T. Gunnlaugsson, A. J. M. Huxley, C. P. McCoy, J. T. Rademacher, T. E. Rice, Chem. Rev. 97 (1997) 1515-1566. DOI: 10.1021/cr960386p

[8] J. J. La Clair, Angew. Chemie - Int. Ed. English 37 (1998) 325-329. DOI: 10.1002/(SICI)1521-3773(19980216)37:3<325::AID-ANIE325>3.0.CO;2-L

[9] S. I. Druzhinin, N. P. Ernsting, S. A. Kovalenko, L. P. Lustres, T. A. Senyushkina, K. A. Zachariasse, J. Phys. Chem. A 110 (2006) 2955-2969. DOI: 10.1021/jp054496o

[10] K. Rotkiewicz, K. H. Grellmann, Z. R. Grabowski, Chem. Phys. Lett. 19 (1973) 315. https://doi.org/10.1016/0009-2614(73)80367-7

[11] M. Segado, I. Gómez, and M. Reguero, Phys. Chem. Chem. Phys., 18 (2016) 6861-6874. DOI: 10.1039/C5CP04690D

[12] K. A. Zachariasse, M. Grobys, Th. von der Haar, A. Hebecker, Yu. V. Il'ichev, Y.-B. Jiang, O. Morawski and W. Kühnle, J Photochem Photobiol A. 102 (1996) 59-70. DOI: 10.1016/S1010-6030(96)04368-7

[13] K. Rotkiewicz, K. H. Grellmann and Z. R. Grabowski, Chem. Phys. Lett. 19 (1973) 212. DOI: 10.1016/0009-2614(73)80367-7

[14] P. B. Coto, L. Serrano-Andrés, T. Gustavsson, T. Fujiwara and E. C. Lim, Phys. Chem. Chem. Phys., 13 (2011) 15182-15188. DOI: 10.1039/c1cp21089k

[15] Andrzej L. Sobolewski, Wolfgang Domcke, Chem. Phys. let. 250 (1996) 428-436. DOI: 10.1016/0009-2614(96)00014-0

[16] J. Dreyer, A. Kummrow, J. Am. Chem. Soc. 122 (2000) 2577-2585. DOI: 10.1021/ja992095e

[17] K. A. Zachariasse, S. I. Druzhinin, V. A. Galievsky, S. Kovalenko, T. A. Senyushkina, P. Mayer, M. Noltemeyer, M. Boggio-Pasqua, M. A. Robb, J. Phys. Chem. A 113 (2009) 2693-2710. DOI: DOI: 10.1021/jp8078925

[18] M. Park, C.H. Kim, T. Joo, J. Phys. Chem. A 117 (2013) 370-377. DOI: 10.1021/jp310842z

[19] I. Fdez. Galván, M. E. Martín, M. A. Aguilar, Chem. Phys. Lett. 499 (2010) 100-102. DOI: 10.1016/j.cplett.2010.09.029

[20] I. Gómez, M. Reguero, M. Boggio-Pasqua and M. A. Robb, *J. Am. Chem. Soc.*, 127 (2005) 7119-7129. DOI: 10.1021/ja042413w

[21] J. M. Rhinehart, R. D. Mehlenbacher, D. W. McCamant, J. Phys. Chem. B 114 (2010) 14646-14656. DOI: 10.1021/jp1023982

[22] J. M. Rhinehart, J. R. Challa, D. W. McCamant, J. Phys. Chem. B 116 (2012) 10522-10534. DOI: 10.1021/jp3020645

[23] A. Perveaux, P. J. Castro, D. Lauvergnat, M. Reguero and B. Lasorne, J Phys Chem Lett 6 (2015) 1316-1320. DOI: 10.1021/acs.jpclett.5b00162

[24] B. F. E. Curchod, A. Sisto, T. J. Martínez, "Ab Initio Multiple Spawning Photochemical Dynamics of DMABN Using GPUs" J. Phys. Chem. A 121 (2017) 265-276. DOI: 10.1021/acs.jpca.6b09962

[25] Frisch, J. M.; Trucks, G. W.; Schlegel H. B.; Scuseria, G. E.; Robb, M. A.; Cheeseman, J. R.; Scalmani, G; Barone, V; Menucci, B.; Petersson, G. A.; et Al. Gaussian 09, revision D. 01; Gaussian, Inc.: Wallingford, CT, 2009

[26] Aquilante, F.; De Vico, L.; Ferré, N.; Ghigo, G.; Malmqvist, P. A.; Neogrády, A.; Bondo Pedersen, T.; Pitoňák, M; Reiher, M.; Roos, B. O.; et al. Software News and Update. MOLCAS 7: The Next Generation. J. Comput. Chem. 31 (2010) 224-247]

[27] O. Vendrell, H.-D. Meyer, J. Chem. Phys. 134 (2011) 044135. DOI: 10.1063/1.3535541

[28] M. H. Beck, A. Jäckle, G. A. Worth, H.-D. Meyer, Phys. Rep. 324 (2000) 1–105. DOI: 10.1016/S0370-1573(99)00047-2

[29] MCTDH web page: http://www.pci.uni-heidelberg.de/cms/mctdh.html

[30] H. Köppel, W. Domcke, L. S. Cederbaum, Adv. Chem. Phys. 57 (1984) 59-246.

[31] L. S. Cederbaum, W. Domcke, J. Chem. Phys. 64 (1976) 603. DOI: 10.1063/1.432250

[32] L. S. Cederbaum, W. Domcke, H. Köppel, W. Von Niessen, Chem. Phys. 26 (1977) 169-177. DOI: 10.1016/0301-0104(77)87041-9

[33] L. Joubert-Doriol, B. Lasorne, F. Gatti, M. Schröder, O. Vendrell, H.-D. Meyer, Comput. Theor. Chem. 990 (2012) 75-89. DOI: 10.1016/j.comptc.2011.12.015

[34] A. Nauts, X. Chapuisat, Mol. Phys. 55 (1985) 1287–1318. DOI: 10.1080/00268978500102031

[35] X. Chapuisat, A. Nauts, J.-P. Brunet, Mol. Phys. 72 (1991) 1–31. DOI: 10.1080/00268979100100011

[36] R. Meyer, Hs. H. Günthard, J. Chem. Phys. 49 (1968) 1510–1520. DOI: 10.1063/1.1670272

[37] M. Harthcock, J. Laane, J. Mol. Spectrosc. 91 (1982) 300-324. DOI: 10.1016/0022-2852(82)90147-3

[38] D. Lauvergnat, A. Nauts. J. Chem. Phys. 117 (2002), 8560–8570. DOI: 10.1063/1.1469019

[39] E. Mátyus, G. Czakó, A.G. Császár, E. Mátyus, G. Czakó, A. Császár, J. Chem. Phys. 130 (2009) 134112. DOI: 10.1063/1.3076742

[40] D. Strobusch, C. Scheurer, J. Chem. Phys. 138 (2013) 94107. DOI: 10.1063/1.4793627

[41] X. Chapuisat, C. Iung, Phys. Rev. A. 45 (1992) 6217–6235. DOI: 10.1103/PhysRevA.45.6217

[42] F. Gatti, C. Muñoz, C. Iung, J. Chem. Phys. 114 (2001) 8275. DOI: 10.1063/1.1361069

[43] F. Gatti, C. Iung, Phys. Rep. 484 (2009) 1–69. DOI: 10.1016/j.physrep.2009.05.003

[44] M. Ndong, L. Joubert-Doriol, H.-D. Meyer, A. Nauts, F. Gatti, D. Lauvergnat, J. Chem. Phys. 136 (2012) 34107. DOI: 10.1063/1.3675163

[45] M. Ndong, A. Nauts, L. Joubert-Doriol, H.-D. Meyer, F. Gatti, D. Lauvergnat, J. Chem. Phys. 139 (2013) 204107. DOI : 10.1063/1.4828729